Hindawi
International Journal of Rotating Machinery
Volume 2022, Article ID 5308514, 15 pages
https://doi.org/10.1155/2022/5308514

Research Article

Film Effectiveness Downstream the Trenches with Tilted Target Wall

Fan Yang and Mohammad E. Taslim

Mechanical and Industrial Engineering Department, Northeastern University, Boston, Massachusetts 02115, USA

Correspondence should be addressed to Mohammad E. Taslim; m.taslim@neu.edu

Received 30 June 2022; Accepted 24 September 2022; Published 7 October 2022

Academic Editor: Funazaki Ken-ichi

Film cooling is a commonly-accepted effective way to protect the gas turbine hot sections from the high temperature products of the combustion chamber. Numerous film hole geometries have been the subject of investigation by many researchers over the past three decades with the aim of keeping the target wall under the maximum allowable temperature with the least amount of precious cooling air and minimum aerodynamic losses. In this study, we are proposing a new trench geometry that is fed by 30°-inclined embedded circular film holes entering from the trench sidewall. The cooling jets impinge on the opposite wall of the trench which is tilted towards the jets and then is pushed over the coverage wall by the main flow. Three trench geometries with the same exit area and tilt angles (the angle between the trench side- and top-wall) of 75°, 90°, and 105° degrees are tested for three blowing ratios of 0.5, 0.75, and 1.0, and the film effectiveness results are compared using the adiabatic pressure sensitive paint technique. CFD analyses are also performed using the realizable $k-\varepsilon$ turbulence model with the enhanced wall function option. Major conclusions of this study were that the trench geometry with the trench tilt angle of 75°, corresponding to the smallest trench volume, had the best performance at the lowest blowing ratio, and good agreement was observed between the CFD and test results.

1. Introduction

To increase the power output and thermal efficiency of gas turbines, the temperature of the combustion chamber products has continuously been increased. This increase, however, has been possible by proper cooling of the turbine hot sections in generals and airfoils in particular in order to maintain the component temperatures below the allowable limits. Among the several commonly-used cooling methods, film cooling of the airfoil external surfaces, exposed to high temperature combustor gases, is an efficient way to create a thermal protection over the airfoil surfaces. Much research is conducted in this area to find a film hole geometry with the highest film effectiveness with the minimum cooling air. Slots, inclined cylindrical holes, conical holes, fan-shaped holes, diffusion holes including the laidback and compound-angle holes, tripod holes, sister-holes, and trenches fed by various film holes have all been investigated experimentally and numerically over the past five decades. The 2D tangential slots [1–2] can provide a uniform and continuous film layer on the target surface. They may, however, compromise the airfoil structural integrity and aerodynamic efficiency. Some studies on discrete film holes include traditional cylindrical holes [3], laidback fan-shaped holes [4–9], tripod holes [10–14], holes with sister holes [10–18], curved diffusion holes [19], and diffusion holes with different exit area geometries [20]. In this paper, we will study a new trench geometry, both experimentally and numerically, and discuss and compare the results. Some previous trench geometry studies close to our proposed trench geometry include that of Waye and Bogard [21] who studied the influence of perpendicular and inclined trench walls with trench depth of 1/2 film hole diameter. They compared nine geometries for various blowing ratios,

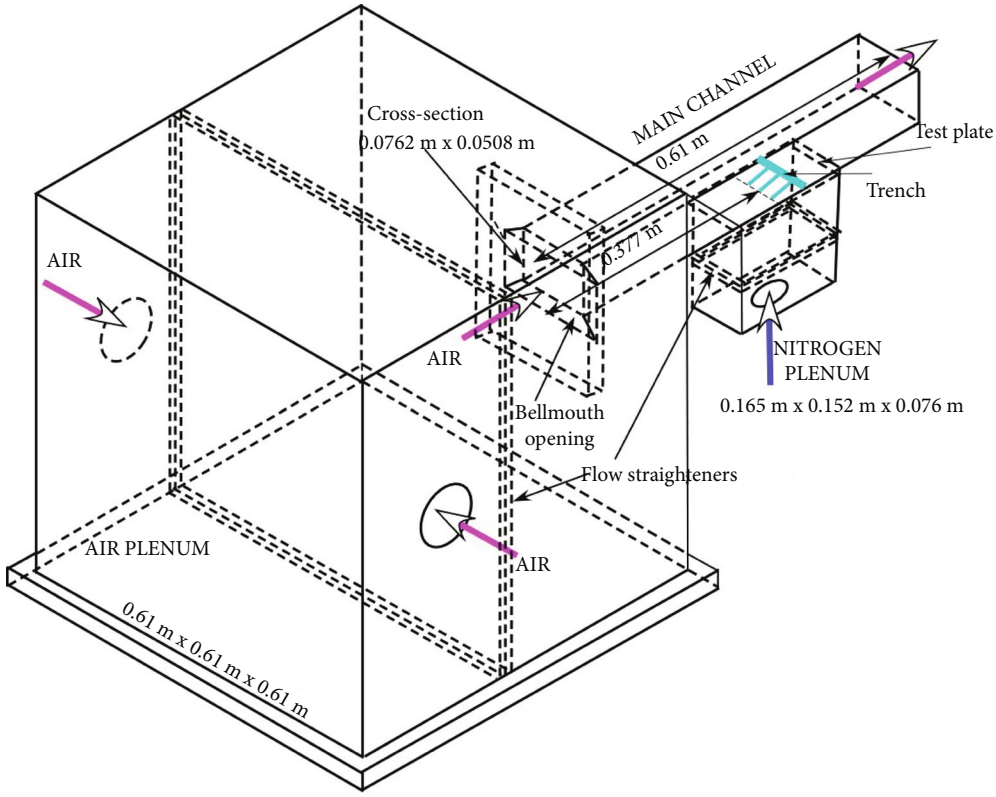

Figure 1: Test rig schematics.

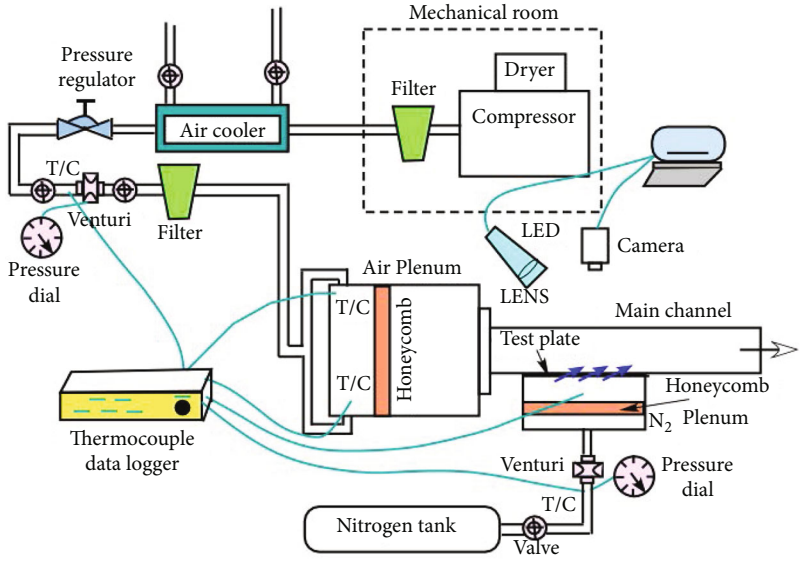

Figure 2: Test rig, associated accessories, and data collection equipment.

density ratios, and freestream turbulence intensities. They concluded that a perpendicular trench wall at the very downstream edge of the coolant hole was found to be the key trench characteristic that yielded much improved adiabatic effectiveness performance. They also pointed out to the fact that, with comparable film effectiveness, trenches are easier and less expensive to manufacture compared with the shaped diffusion holes.

Basic parameters of trench geometries such as width and depth were studied by Lu et al. [22]. Their results show that film effectiveness is greatly enhanced by the trenching due to the improved two-dimensional nature of the film and lateral spreading. The optimum trench depth of 0.75 d was confirmed by both of their experimental and CFD results.

Oguntade et al. [23] tested several trench geometries with fixed depth of 0.75 d and nominal opening of 2 d. They,

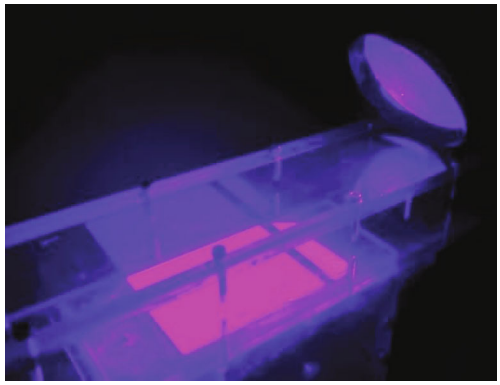

Figure 3: Test plate with LED light on.

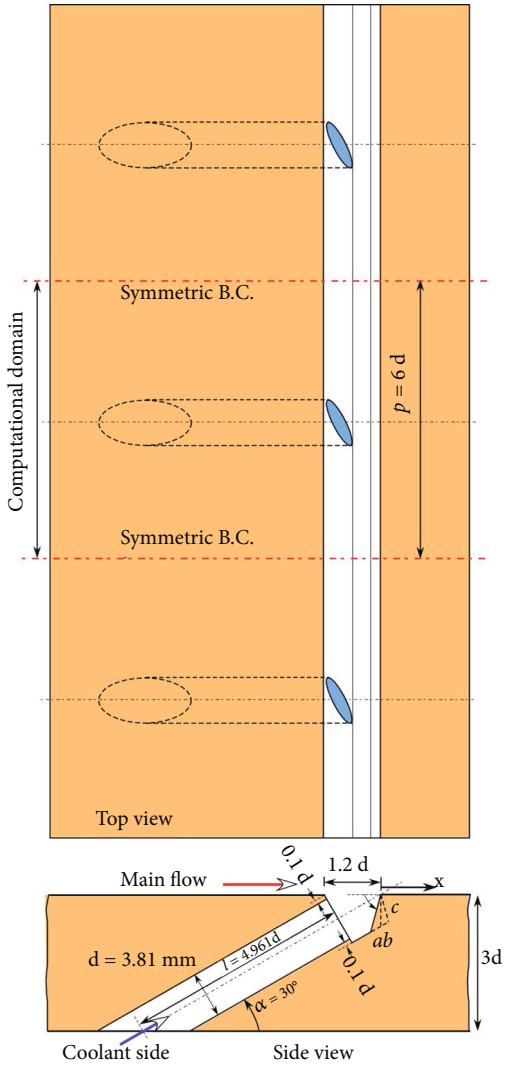

Figure 4: Details of the film cooling holes and trench geometry.

however, chamfered and rounded the tip of the trench exit wall to improve the coolant attachment to the downstream surface. They concluded that the Coanda effect around the trench wall exit caused the attachment of the coolant to

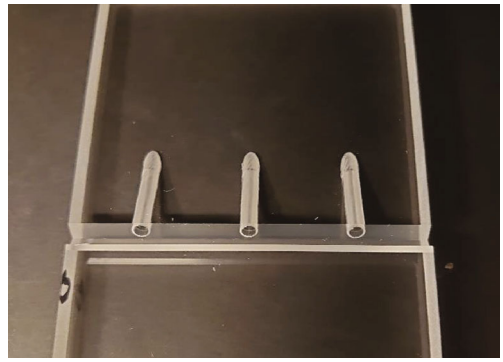

Figure 5: Machined Geometry *a*.

Figure 6: A black and white image of light intensity downstream of the trench.

the downstream area with improved film cooling effectiveness.

Wei et al. [24] designed and measured the performance of cylindrical holes embedded in a sine-wave shaped trench. Anticounter-rotating vortices were observed to help with the spanwise spreading of coolant in their geometry. The conclusion was that, compared with traditional transverse trenches, the sine-wave shaped trenches faced less flow resistance and provided higher film cooling effectiveness, and the sinewave trenches with higher amplitude could exhibit better performance at low blowing ratios.

Barahate and Vedula [25] measured the film cooling effectiveness of a single row of holes embedded in an inclined trench. Their cylindrical film holes were perpendicular to the mainstream and entered the 35°-inclined trench along its bottom surface. Three pitch-to-diameter ratios of 3, 4.5, and 6 were tested. Their major conclusion was that, at higher blowing ratios, the effectiveness values for their inclined trenches were higher whereas the heat transfer coefficients were smaller, compared to those of the normal trenches.

Recently, Song et al. [26] reported on the combination of trench and fan-shaped holes. Results showed that the film effectiveness increased especially when the downstream trench wall was closer to the film hole exit. Wu et al. [27] studied film cooling performance of 30°-inclined round holes embedded in various crater and trench geometries

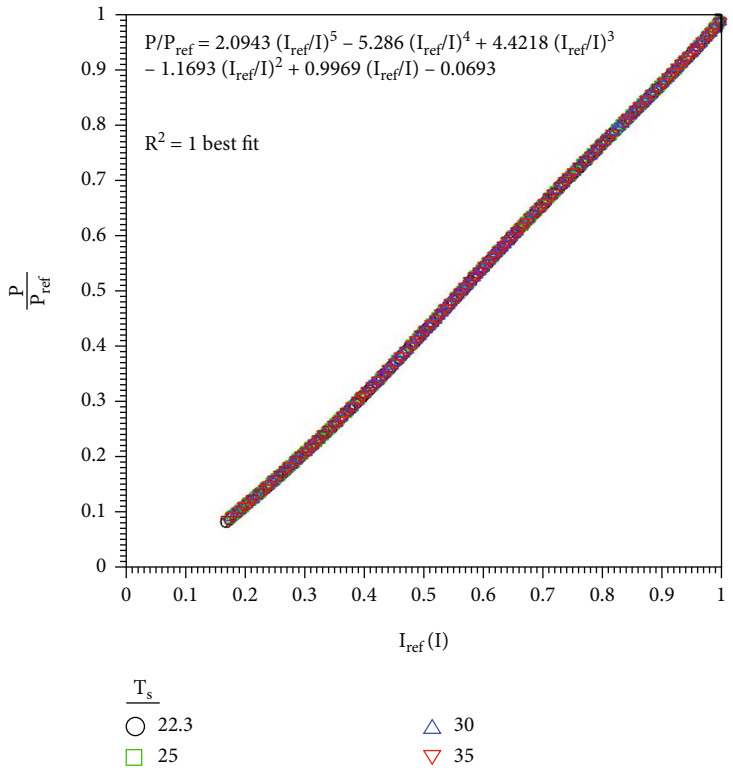

Figure 7: Calibration curve at different temperatures: 22.3, 25, 30, and 35°C.

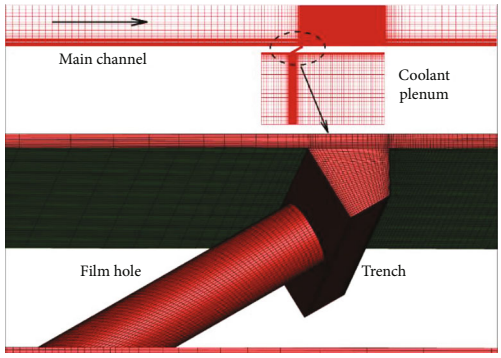

Figure 8: Mesh details for Geometry *b* around the trench and feed hole.

(transverse, W-shaped, and elliptic). Major conclusions of this study were that, with the same depth and width, W-shaped trenches improved the lateral spreading of coolant and generated higher cooling effectiveness, compared to the transverse trenches, elliptic trenches exhibited the worst cooling performance, and the increase in trench depth and decrease in trench width resulted in an increase in the discharge coefficient. Bahambari et al. [28] performed a numerical study on the w-wave trenches of amplitudes 5, 10, and 15. 30°-inclined cylindrical film holes with $p/d = 3$ entered the wavy trenches along the bottom surface. They concluded that the wave geometry with an amplitude of 10 performed relatively better than the other two amplitudes and produced 23% higher laterally-averaged film cooling effectiveness than the transverse trench at a blowing ratio of 2. Our new proposed trench geometry aimed at increasing the film cooling effectiveness with minimum loss of coolant momentum. The coolant jet entering the trench on its sidewall is position such that almost half of the coolant strikes the opposite tilted trench wall and moves to the edge while the other half will directly shoot into the main flow at the trench exit plane. These two coolant streams, in combination, are believed to have a more effective coverage of the target surface. Three trench wall tilt angles are tested at three blowing ratios of 0.5, 0.75, and 1 using the pressure sensitive paint (PSP) technique. For the CFD analyses, the Fluent™ solver along with the realizable $k - \varepsilon$ turbulence model with the enhanced wall function option was used.

2. Experimental Setup

Figures 1 and 2 show the experimental setup. An air compressor provided the main flow while the coolant was supplied by a compressed nitrogen tank. Two critical venturimeters, choked at all flow conditions, measured the air and nitrogen flow rates. Air and nitrogen plenums, main flow channel, and test plates were made of 0.127 cm thick clear acrylic plastic slabs. Both air and nitrogen plenums were equipped with aluminum honeycomb flow-straighteners to deliver a uniform flow to the main flow channel and to the film holes. K-type thermocouples were connected before and after the venture meters to collect the temperature data by the acquisition system. The removable test piece with three film holes was installed between the test channel and

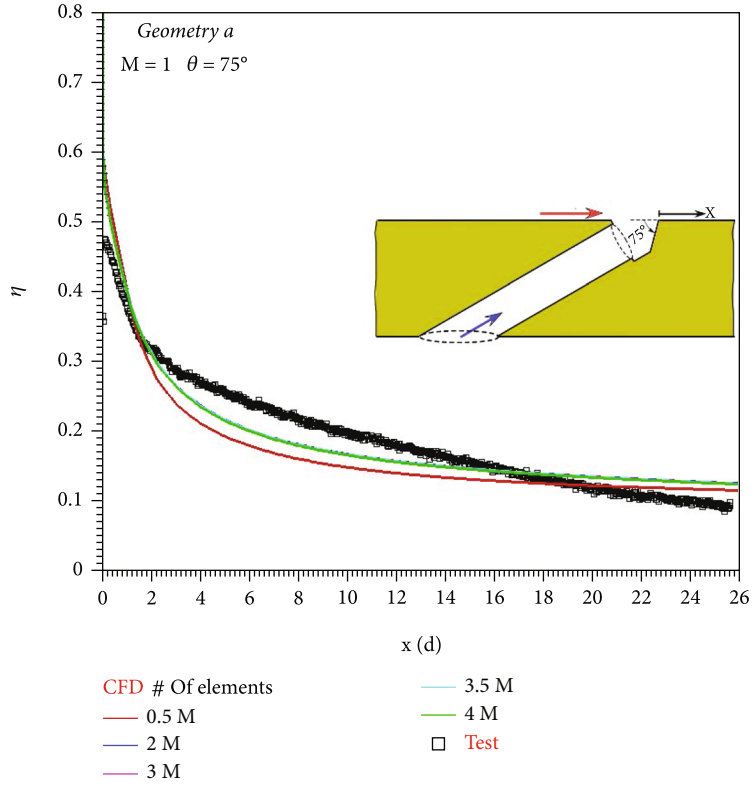

Figure 9: Mesh independence results.

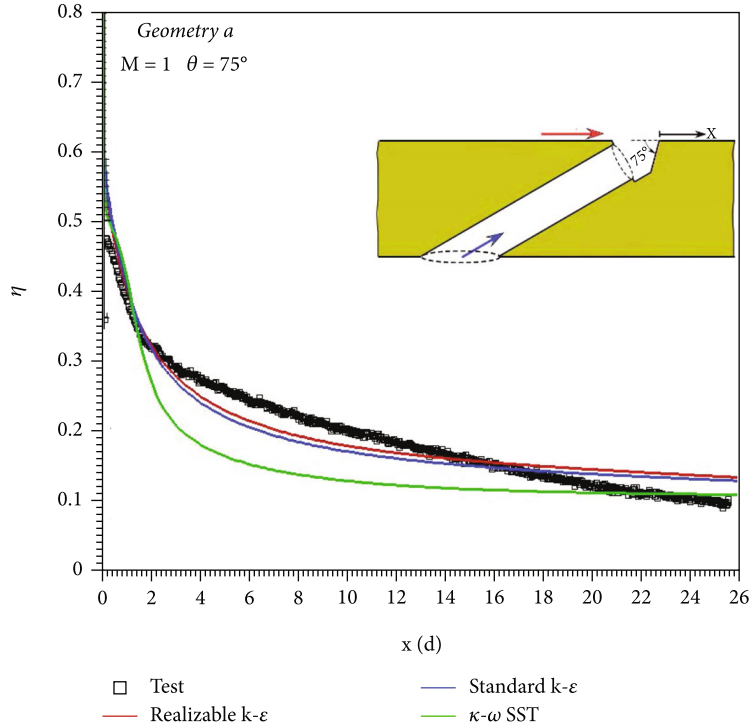

Figure 10: Comparison of different turbulence models with the test results.

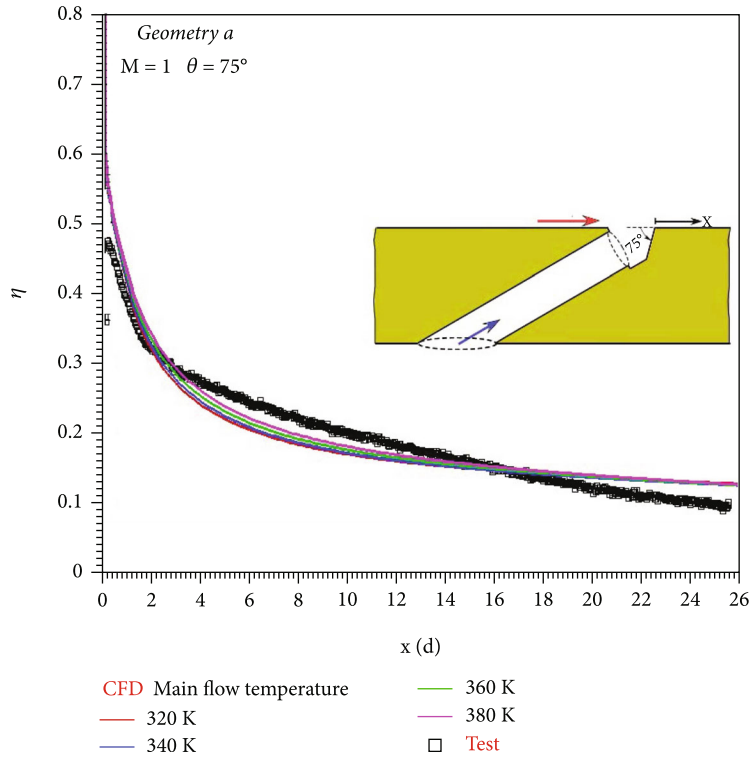

Figure 11: Main flow temperature setting effects on CFD results.

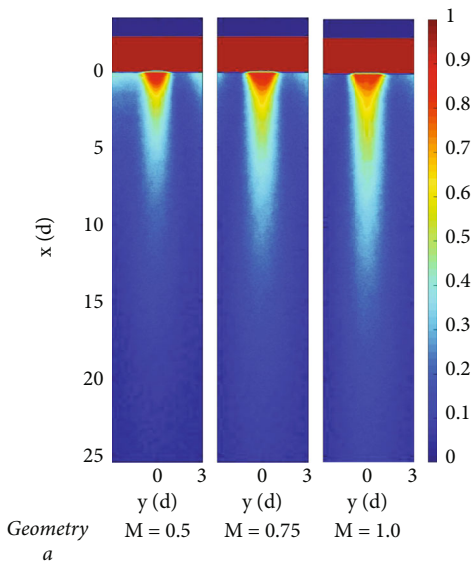

Figure 12: Experimental contours of film effectiveness for Geometry *a*.

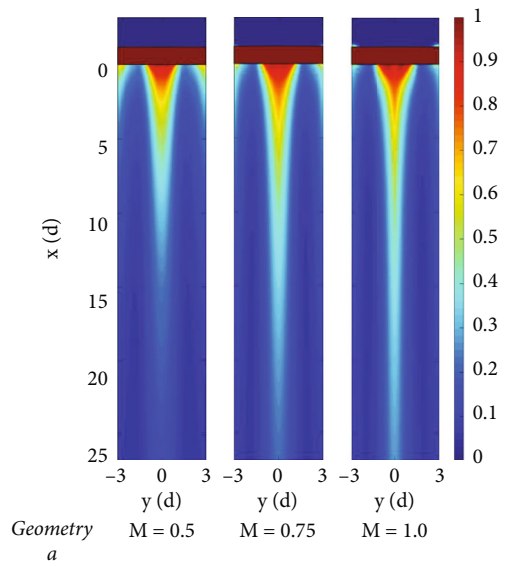

Figure 13: CFD contours of film effectiveness for Geometry *a*.

coolant plenum. The reported data in all geometries are for the middle hole to eliminate any side effects. A 1600 by 1200-pixel CCD camera (ImageSource, DMK 23U274) with a 610 nm light filter was installed above the test channel perpendicular to the test piece. The camera was controlled by a computer with IC Measure. A 400 nm ultraviolet LED light (Thorlabs, M405L3 Mounted LED) was set beside the camera to excite the pressure-sensitive paint. Figure 3 shows a typical test light setup.

The trench with a cross-sectional area similar to that of a rain gutter, shown in Figure 4, is fed by circular film holes, each at an inclination angle of $\alpha = 30\circ$. These holes are positioned such that the coolant jet nearly divides into two streams the lower half of which strikes the trench wall and rebounds and then gets pushed over the target surface by

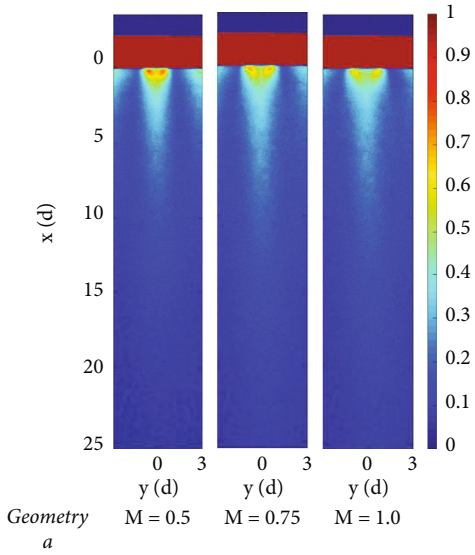

Figure 14: Experimental contours of film effectiveness for Geometry *b*.

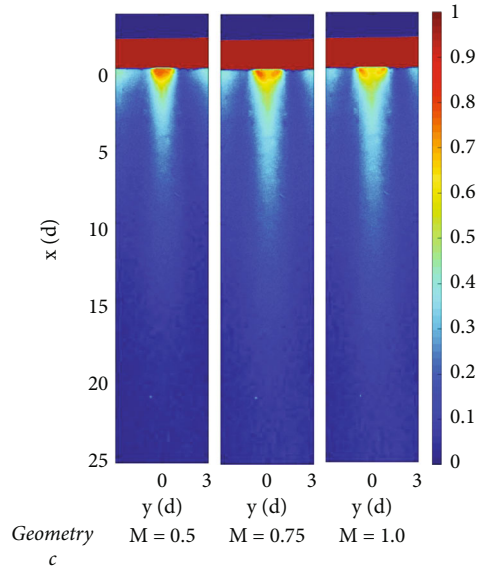

Figure 16: Experimental contours of film effectiveness for Geometry *c*.

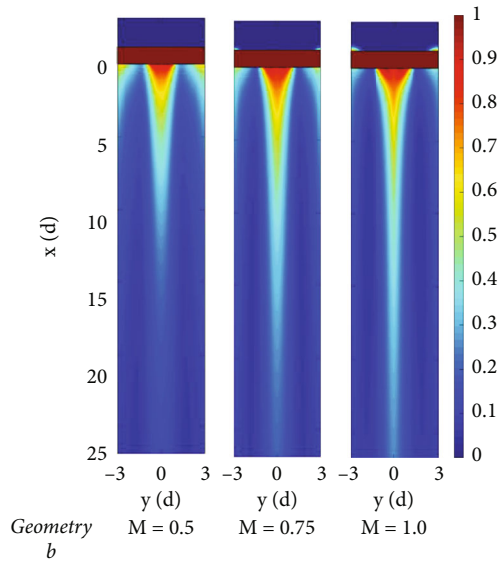

Figure 15: CFD contours of film effectiveness for Geometry *b*.

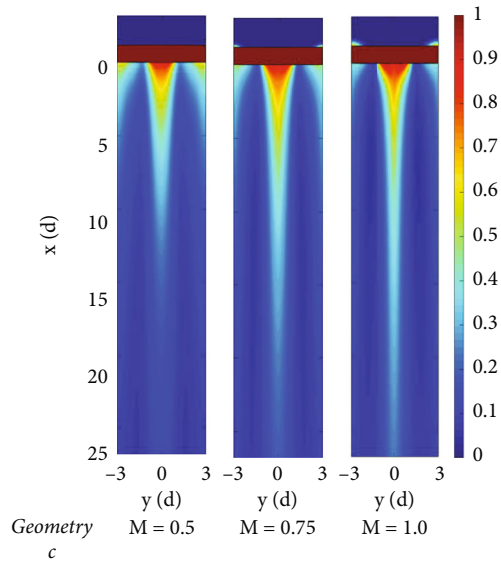

Figure 17: CFD contours of film effectiveness for Geometry *c*.

the remaining half of the coolant. Three trench wall tilt angles, $\theta = 75\circ$, 90°, and 105°, shown in Figure 4 (side view), were tested. These geometries are called *a*, *b*, and *c* in this paper. Three test pieces corresponding to geometries *a*, *b*, and *c* were modelled in SoldWorks™ and machined out of clear acrylic plastic at Northeastern University machine shop. On each piece, three identical film holes, separated by a center-to-center distance (pitch) of 6 d, supplied the coolant to one longitudinal trench. The reported data is for the coverage area downstream of the middle hole so that the edge effects were eliminated. Different from the commonly-used trench geometries with wide-open exit areas, the proposed geometry in this work optimizes the exit area and trench space which could result in less aerodynamic losses and more structural strength for the airfoils. As the trench wall tilt angle, θ, increases, the trench space increases. One of the objectives of this study is to investigate the influence of the trench target wall orientation on the coolant distribution and film effectiveness. Figure 5 shows the machined test piece geometry for Geometry *a* ($\theta = 75\circ$) before being sprayed with the pressure sensitive paint.

2.1. PSP Calibration and Test Uncertainties. The pressure sensitive paint (PSP) technique which is conducted under isothermal conditions was first presented by Navarra et al. [29]. Compared with the temperature sensitive paint (TSP)

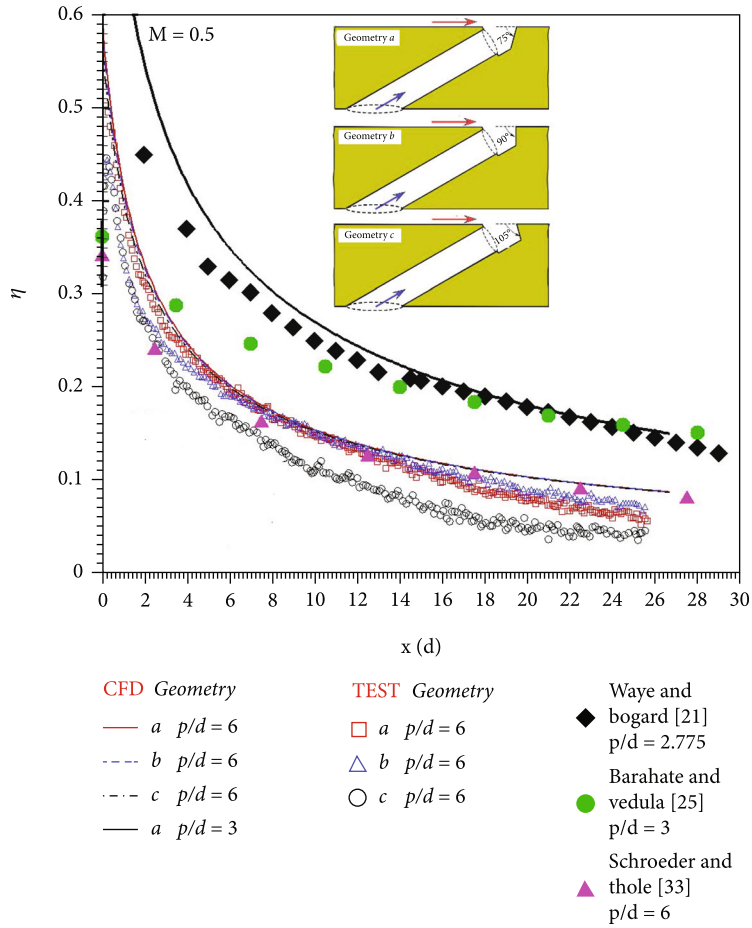

Figure 18: Spanwise-averaged film effectiveness in the streamwise direction for the blowing ratio of $M = 0.5$.

and infrared (IR) techniques, there is little to no heat losses in the PSP tests thus no uncertainty associated with possible heat losses enters the data reduction process. Furthermore, conventional measurement techniques called for the use of many thermocouples for a proper film effectiveness data collection and limited number of thermocouples at discrete points on the target surface did not accurately produce a continuous thermal image of that area. This shortcoming, compounded by the number of leads and thermal losses associated with them, increased the overall experimental uncertainty. The PSP method, however, produces a continuous image of the film cooling effectiveness (illuminance intensity) with high resolution over the entire surface under investigation. In this study, The UniFIB® pressure sensitive paint and FIB Basecoat™ from ISSI Innovative Solutions Inc. were used. When a UV light source (a 400 nm ultraviolet LED through a convex lens with 15 cm focal length, in this study) is cast on the painted surface, the paint illuminates with varying intensity depending on the partial pressure of the surrounding oxygen. Figure 6 shows a black and white image of light intensity downstream of the trench. Under identical boundary conditions (impermeable wall versus adiabatic wall), analogy between the mass and energy transport equations reveals that the film cooling effectiveness can be recast into

$$\eta = \frac{C_{aw} - C_\infty}{C_c - C_\infty} = 1 - \frac{1}{1 + \left(\left(P_{O_2,\text{air}}/P_{O_2,\text{mix}}\right) - 1\right)\left(M_{N_2}/M_{\text{air}}\right)}. \quad (1)$$

The intensity ratio which is a function of the oxygen partial pressure can be modelled as

$$\text{IR} = \frac{I_{\text{ref}} - I_{\text{black}}}{I - I_{\text{black}}} = f\left(\frac{P}{P_{\text{ref}}}\right) = f\left(P_{O_2}\right). \quad (2)$$

First, the PSP had to be calibrated in a vacuum chamber to determine a functional relationship between the luminescence and the oxygen partial pressure. Calibration data representing the functional dependence of luminescence with the oxygen partial pressure at different surface temperatures are shown in Figure 7, and details of the calibration setup are given in Baldino and Taslim [30]. Throughout this study, for film effectiveness evaluation, a 5th-degree polynomial representing the best fit to the data was used.

Each test started with setting the main flow (air) to the fixed value of 0.1016 kg/s corresponding to a Reynolds

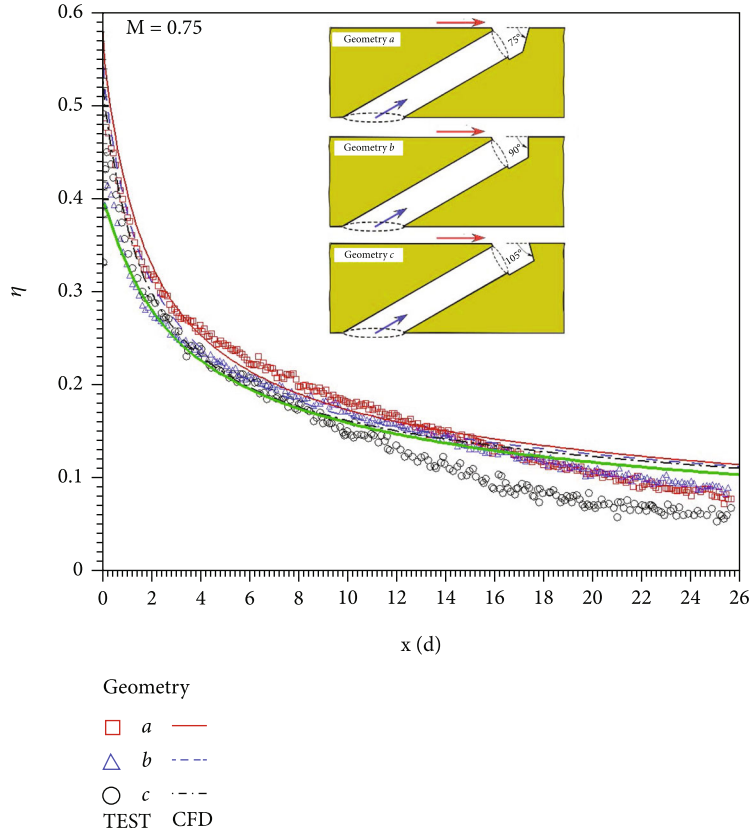

Figure 19: Spanwise-averaged film effectiveness in the streamwise direction for the blowing ratio of $M = 0.75$.

number of 87200, without any coolant running. In all tests, the main flow, the coolant, and the test section were all at the same temperature as that of the lab temperature; thus, there was no heat transfer through the test piece. Once the system reached equilibrium, proper lighting was set and a baseline photo was captured to serve as the reference light intensity to which all captured photos during a film cooling effectiveness test were compared. The coolant (nitrogen) mass flow rate was then set to a predetermined value corresponding to the desired blowing ratio. The main flow and coolant mass flow rates, divided by the main channel and the film hole inlet cross-sectional areas, respectively, gave the $(\rho U)_{\text{air}}$, $(\rho U)_{N_2}$, and the blowing ratio.

$$M = \frac{(\rho U)_{N_2}}{(\rho U)_{\text{air}}} = \frac{\dot{m}_{N_2}/(\pi/4)d^2}{\dot{m}_{\text{air}}/A_{\text{passage}}}. \tag{3}$$

The freestream turbulence intensity in the main channel was measured to be 3.86%.

As for the measurement uncertainties, the vacuum pressure measurement sensor was found to be the main source of uncertainty. Since each test takes only a few minutes, the decay of PSP becomes insignificant [31]. Errors associated with the LED lighting and CCD camera as well as the slight temperature variations are insignificant. Following the method of Kline and McClintock [32], the uncertainty in film cooling effectiveness can be expressed as

$$\delta\eta = \sqrt{\left(\frac{\partial\eta}{\partial P_{O_2}}\right)^2 \delta P_{O_2}^2}, \tag{4}$$

where the derivative term in the above equation is determined from Equation (1) is

$$\frac{\delta\eta}{\delta P_{O_2}} = -\frac{\left(M_{N_2}/M_{\text{air}}\right)21.21}{\left(\left(\left(M_{N_2}/M_{\text{air}}\right)21.21/P_{O_2}\right) + 1 - \left(M_{N_2}/M_{\text{air}}\right)\right)^2 P_{O_2}}. \tag{5}$$

21.21 is the mole fraction of oxygen in air. The vacuum pressure sensor accuracy, δP, specified by the manufacturer, depends on the measured pressure

$$\begin{cases} \text{if } P < 50 \text{ kPa} \longrightarrow \delta P = \pm 10\% \text{ of reading}, \\ \text{if } P > 50 \text{ kPa} \longrightarrow \delta P = \pm 2.5\% \text{ of reading}. \end{cases} \tag{6}$$

The uncertainty of the oxygen partial pressure $(\delta P_{O2})\delta P_{O2})$ is given by the uncertainty of the absolute pressure

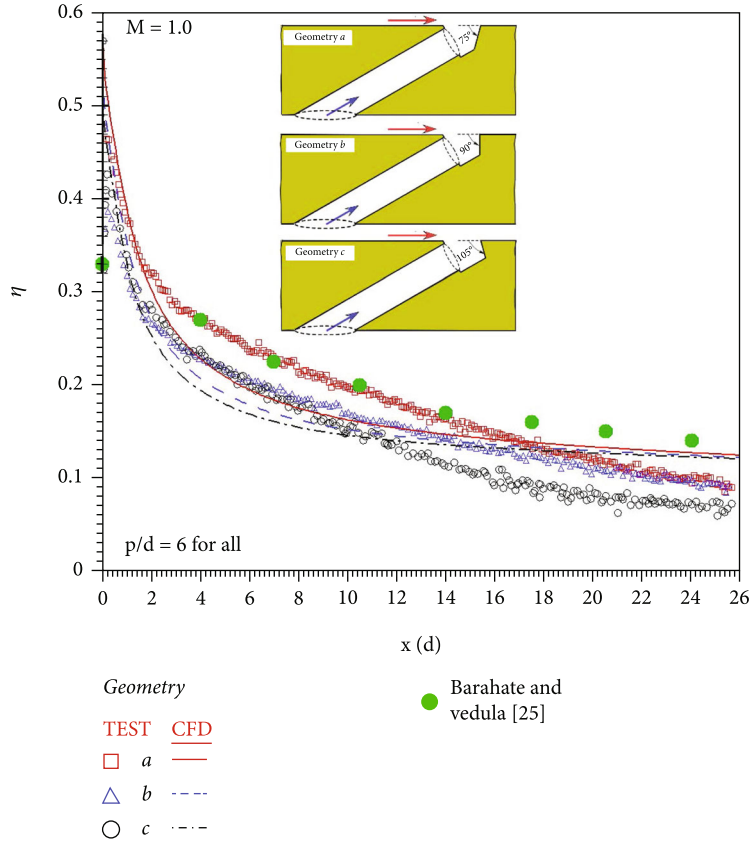

Figure 20: Spanwise-averaged film effectiveness in the streamwise direction for the blowing ratio of $M = 1$.

times the oxygen concentration percentage within the air.

$$\begin{cases} \delta P_{O_2} = 0.21\delta P = 0.10 P_{O_2} & \text{if } P < 50 \text{ kPa}, \\ \delta P_{O_2} = 0.21\delta P = 0.025 P_{O_2} & \text{if } P > 50 \text{ kPa}. \end{cases} \quad (7)$$

In conclusion, the film effectiveness maximum uncertainty was calculated to be about ±5%. More details of the uncertainty analysis are discussed in Baldino and Taslim [30].

2.2. Numerical Analyses. For each geometry, a representative CFD model, made up of the main channel, the coolant plenum, the middle film hole, and its center-to-center share of the trench, was created in SolidWorks™ and was meshed in the powerful ICEM-CFD™ mesher by Ansys. These models were meshed with hexahedral elements, a preferred type of cells for CFD analyses, by their entirety. To capture viscous as well as thermal effects on the boundaries, much finer meshes were arranged on the boundaries, and mesh size was increased from the boundaries to the computational domain core. The two spanwise cut-planes on the two sides of the model were set to the symmetric type to eliminate any edge effects. A typical computational domain with mesh distribution details around the film hole and trench as well as the two symmetric sidewalls is shown in Figure 8. For the solver, Fluent/UNS by Ansys, Inc., a pressure-correction based, multiblock, multigrid, unstructured/adaptive solver, was used.

Mesh independence was achieved at 2 million-mesh level as is shown in Figure 9. Although no significant change was detected in results for mesh sizes beyond this level, we performed all numerical runs with 4 million-mesh models.

Coolant and main flow mass flow rates, exactly the same as those in the tests for different blowing ratios, were specified in the numerical models. Outlet pressures, the same as those of lab pressure when the tests were run, were specified for the CFD runs. The turbulence intensity in the main channel was set to the measured value of 3.86% with a hydraulic diameter of 0.061 m and a fixed Reynolds number of 87200. The boundary layer thickness in the main channel, where film cooling effectiveness was measured, was calculated to be around 5 d so that the coolant was not disturbing its development. For closure, three turbulence models were tested—standard $k-\varepsilon$, realizable $k-\varepsilon$, and $k-\omega$ SST. Figure 10 shows the spanwise-averaged streamwise film effectiveness variation downstream of the trench in the main flow direction for the Geometry *a* for the blowing ratio of 1.0. Comparing the experimental data with the CFD results of the three turbulence models, the realizable $k-\varepsilon$ model with the enhanced wall function option was chosen for all reported CFD results. The y^+ values corresponding to the first layer of cells on the target area were controlled to be below 5 for all geometries.

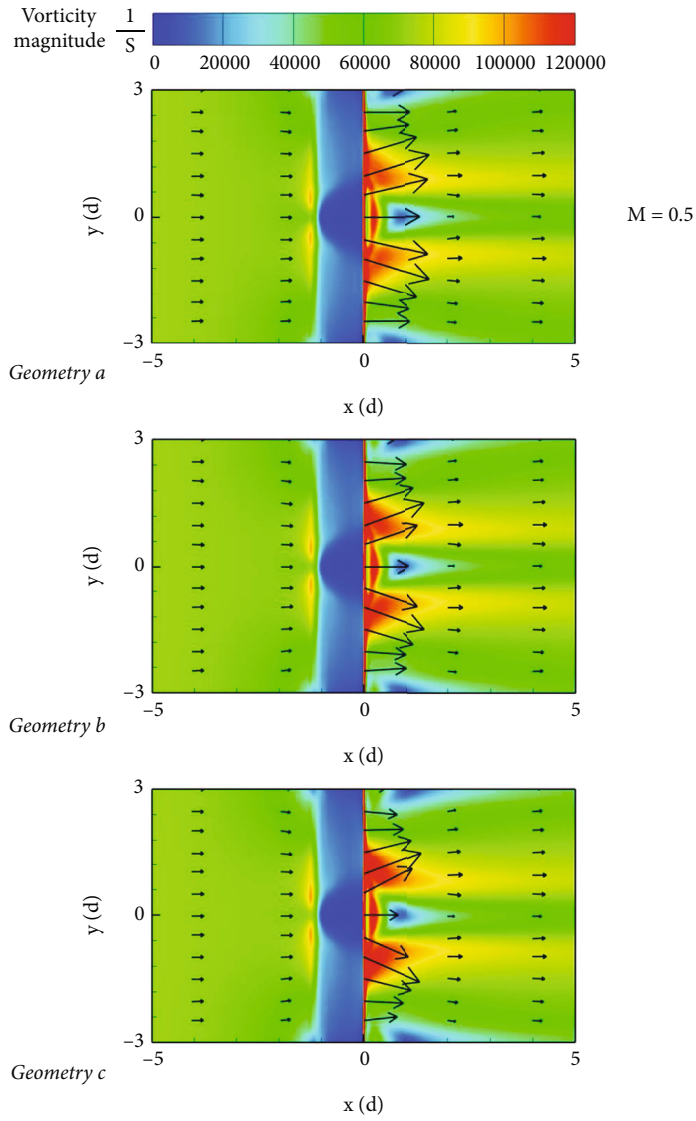

Figure 21: Velocity vectors and vorticity contours for $M = 0.5$.

The coolant temperature in all CFD runs was set to 300 K, while four temperatures of 320 K, 340 K, 360 K, and 380 K for the mainstream temperature, corresponding to temperature differences of 20 K, 40 K, 60 K, and 80 K between the coolant and main flow, were tried with, as expected, no significant change in the film effectiveness results, shown in Figure 11. These runs were for Geometry *a* and a blowing ratio of 1. The remaining CFD cases were run for 20 K temperature difference, and adiabatic condition was set for all walls. Convergence, for most cases, was achieved at around 30,000 iterations with residual sums of all variables less than 1×10^{-7}.

3. Results and Discussions

Figures 12–17 depict the experimental and numerical film effectiveness distribution downstream the middle hole for the three trench geometries and the three blowing ratios. The overall agreement between the test data and numerical results is reasonable. Better coverage is noticed as the blowing ratio increases (from left to right in each figure). This is expected as coolant with higher momentum at higher blowing ratios penetrates into the main flow more effectively and produces a better coverage.

Figures 18–20 show the spanwise-averaged film effectiveness in the streamwise direction. Each figure which represents a blowing ratio compares the test data and numerical results for the three geometries. On Figure 18, we have added the test data of Waye and Bogard [21] for 30°-slanted circular film holes feeding the trench on its floor. They tested this film hole geometry for a much smaller pitch of $p/d = 2.775$, compared to our geometry of $p/d = 6$, and that is the reason for their higher film effectiveness results. We, however, ran a CFD case of our Geometry *a* for a p/d

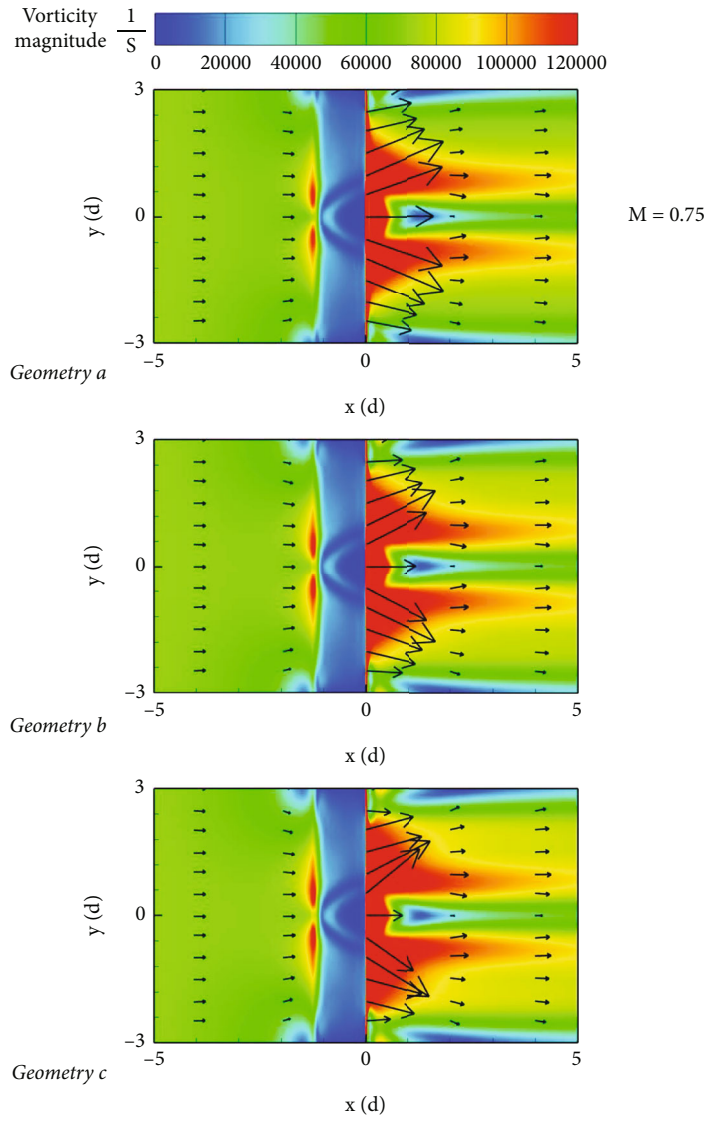

Figure 22: Velocity vectors and vorticity contours for $M = 0.75$.

of 3 to show how close the results of our Geometry *a* are with their data. Two more comparisons with literature data for the same blowing ratio of 0.5 are made—the test data of Barahate and Vedula [25] who tested normal circular film holes entering the bottom of a 35°-inclined trench. Again, given that they had a pitch to diameter ratio of 3 or twice as many feed holes as in our geometry, the results are in reasonable agreement with those of our Geometry *a*. The third set of data for comparison are those of Schroeder and Thole [33] for 7°-7°-7° diffusion film holes at $p/d = 6$ and blowing ratio of 0.5 to show that for the same amount of cooling flow, our proposed trench geometries are as effective as the laid-back discrete diffusion film holes. The numerical results generally agree with the experimental date. As the trench wall tilt angle increases from 75° to 105°, all geometries show a decrease in their film effectiveness. This means, rebound of the coolant in the trench after striking the opposing trench wall will decrease the overall cooling effect. In the 75° tilt angle geometry, the trench wall acting like a ramp leads the coolant over the coverage surface resulting in a more effective cooling.

Figures 21–23 show the velocity vectors and vorticity contours around the trench exit for the three trench geometries, each for the three tested blowing ratios. The contours are on a horizontal plane 0.01 d above the coverage surface. The level of vorticity and the magnitude and direction of the velocity vectors immediately downstream the trench indicate how effective the film cooling is. For example, in Geometry *c* for all blowing ratios, the coolant is forced away and lifted from the coverage area due to the presence of strong vortices downstream the trench which resulted in the lowest film effectiveness as shown in Figures 18–20. For the same reason, Geometry *a* performed better and Geometry *b* fell in between the other two.

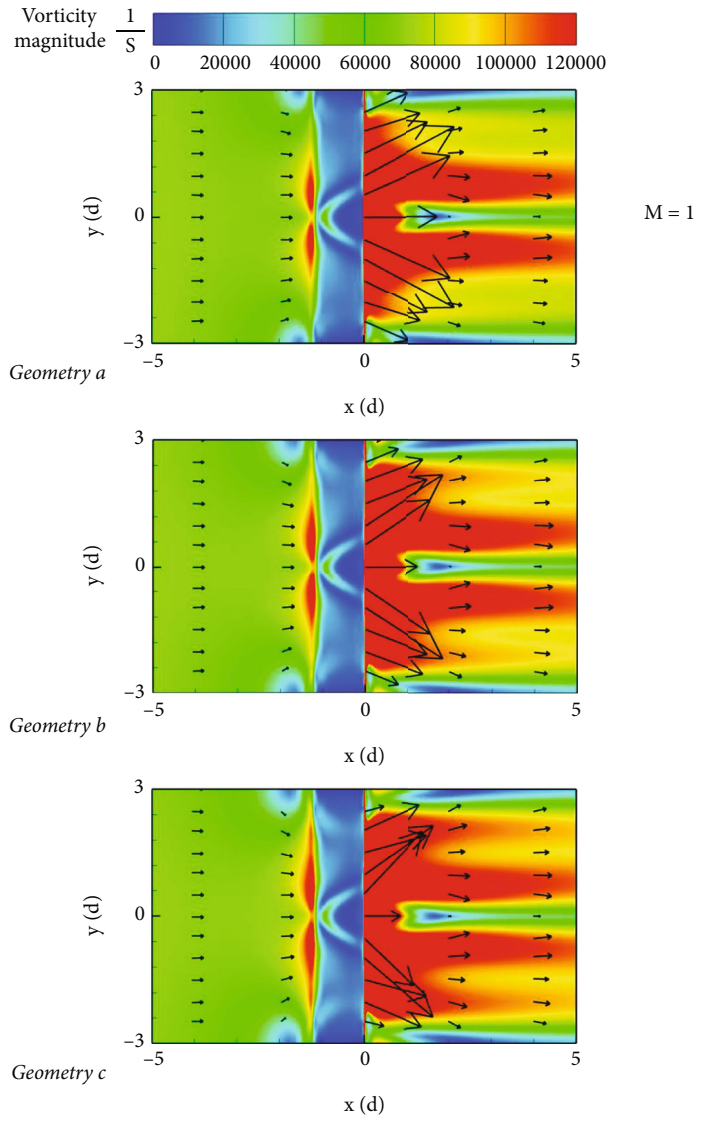

Figure 23: Velocity vectors and vorticity contours for $M = 1$.

4. Conclusions

The film cooling performance of a new trench film cooling geometry was investigated both experimentally and numerically. The influences of blowing ratio and trench downstream wall tilt angle were discussed. Main conclusions are

(1) Geometry *a* corresponding a trench wall tilt angle of 75° produced the best film coverage while Geometry *c* with a trench wall tilt angle of 105° created a severe coolant rebound at the trench exit and consequently a lower film effectiveness

(2) At blowing ratios less than 0.75, the film effectiveness results of our proposed trench geometries are higher than those of the 7°-7°-7° diffusion film holes. With their ease of manufacturing, these trench geometries could be superior to discrete diffusion holes

(3) Presented test data were for pitch to diameter ratio of 6. Our numerical results, however, showed that a smaller pitch such as 3 d will improve the performance, of course at the expense of more precious coolant

Nomenclature

$A_{passage}$: Main flow passage area (38.71 cm^2)
C: Chemical concentration (%)
d: Feed hole diameter (Figure 4) (3.81 mm)
D_h: Main passage hydraulic diameter (60.96 mm)
I: Light intensity (pixel intensity value)
IR: The ratio of reference light intensity and measured intensity
k: Turbulent kinetic energy
ℓ: Feed hole length (Figure 4, 4.961 d)
$\dot{m}_{N_2}$: Nitrogen mass flow rate per film hole (kg/s)

$\dot{m}_{air}$: Main channel air mass flow rate (0.1016 kg/s)
M: Blowing ratio $(\dot{m}_{N_2}/(\pi d^2/4))/(\dot{m}_{air}/A_{passage})$
M_{N_2}: Coolant molecular weight (28 kg/kmol)
M_{air}: Mainstream (air) molecular weight (28.97 kg/kmol)
p: Hole pitch (6 d = 22.86 mm)
P: Pressure (Pa)
PSP: Pressure-sensitive paint
$P_{O2,air}$: Oxygen partial pressure in main channel approach air (Equation (1), 21 kPa)
$P_{O2,mix}$: Oxygen partial pressure at a given point downstream the film holes (Equation (1) kPa)
Re: Reynolds number based on the passage hydraulic diameter $\rho U D_h/\mu = 87200$
T: Temperature
TSP: Temperature-sensitive paint
U: Main passage air velocity (m/s)
α: Feed hole inclination angle (30°, Figure 4)
ε: Energy dissipation rate per unit mass
η: Film cooling effectiveness
μ: Air dynamic viscosity (kg/(m·s))
θ: Trench wall tilt angle (75°, 90°, and 105° for the three tested geometries, Figure 4)
ρ: Air density (kg/m^3).

Subscripts

aw: Adiabatic wall
blk: Black
c: Coolant
O_2: Diatomic oxygen
N_2: Nitrogen
ref: Reference
∞: Channel mainstream.

Data Availability

Data files are available upon request.

Conflicts of Interest

The authors declare that they have no conflicts of interest.

Acknowledgments

All funds were internal.

References

[1] J. E. Hatch and S. S. Papell, *Use of a theoretical flow model to correlate data for film cooling on heating an adiabatic wall by tangential injection of gases of different fluid properties*, National Aeronautics and Space Administration, 1959.

[2] R. J. Goldstein, "Film cooling," *Advances in Heat Transfer*, vol. 7, pp. 321–379, 1971.

[3] V. L. Eriksen and R. J. Goldstein, "Heat transfer and film cooling following Normal injection through a round hole," *Journal of Engineering for Power*, vol. 96, no. 4, pp. 329–334, 1974.

[4] K. D. Lee and K. Y. Kim, "Surrogate based optimization of a laidback fan-shaped hole for film-cooling," *International Journal of Heat and Fluid Flow*, vol. 32, no. 1, pp. 226–238, 2011.

[5] A. Zamiri, S. J. You, and J. T. Chung, "Large eddy simulation in the optimization of laidback fan-shaped hole geometry to enhance film-cooling performance," *International Journal of Heat and Mass Transfer*, vol. 158, article 120014, 2020.

[6] M. Fraas, T. Glasenapp, A. Schulz, and H. J. Bauer, "Film cooling measurements for a laidback fan-shaped hole: effect of coolant crossflow on cooling effectiveness and heat transfer," *Journal of Turbomachinery*, vol. 141, no. 4, 2019.

[7] M. Fraas, T. Glasenapp, A. Schulz, and H. J. Bauer, "Optimized inlet geometry of a laidback fan-shaped film cooling hole - Experimental study of film cooling performance," *International Journal of Heat and Mass Transfer*, vol. 128, pp. 980–990, 2019.

[8] D. W. Chen, H. R. Zhu, C. L. Liu, H. T. Li, B. R. Li, and D. Zhou, "Combined effects of unsteady wake and free-stream turbulence on turbine blade film cooling with laidback fan-shaped holes using PSP technique," *International Journal of Heat and Mass Transfer*, vol. 133, pp. 382–392, 2019.

[9] H. J. Seo, Y. J. Kang, H. C. Lee, J. S. Kwak, J. S. Park, and K. D. Lee, "Optimization of the configuration of the laidback fan-shaped film cooling hole with a lateral expansion angle of 10 degrees," *Applied Thermal Engineering*, vol. 153, pp. 379–389, 2019.

[10] S. Ramesh, D. G. Ramirez, S. V. Ekkad, and M. A. Alvin, "Analysis of film cooling performance of advanced tripod hole geometries with and without manufacturing features," *International Journal of Heat and Mass Transfer*, vol. 94, pp. 9–19, 2016.

[11] Z. Chi, J. Ren, H. Jiang, and S. Zang, "Geometrical optimization and experimental validation of a tripod film cooling hole with asymmetric side holes," *Journal of Heat Transfer*, vol. 138, no. 6, article 061701, 2016.

[12] S. Ramesh, C. N. LeBlanc, D. Narzary, S. V. Ekkad, and M. A. Alvin, "Film cooling performance of tripod antivortex injection holes over the pressure and suction surfaces of a nozzle guide vane," *Journal of Thermal Science and Engineering Applications*, vol. 9, no. 2, article 021006, 2017.

[13] C. N. LeBlanc, S. Ramesh, S. V. Ekkad, and M. A. Alvin, "Effect of Hole Exit Shaping on Film Cooling Performance for Tripod Hole Injection over a Flat Surface," in *Proceedings of the ASME Turbo Expo 2013: Turbine Technical Conference and Exposition. Volume 3B: Heat Transfer*, San Antonio, Texas, USA, 2013.

[14] Z. Chi, J. C. Han, X. Li, J. Ren, and H. Jiang, "Geometrical Optimization and Experimental Validation of a Tripod Film Cooling Hole with Asymmetric Side Holes," *Turbo Expo: Power for Land, Sea, and Air*, vol. 45721, 2014.

[15] M. J. Ely and B. A. Jubran, "A numerical evaluation on the effect of sister holes on film cooling effectiveness and the surrounding flow field," *Heat and Mass Transfer*, vol. 45, no. 11, pp. 1435–1446, 2009.

[16] M. J. Ely and B. A. Jubran, "Film cooling from short holes with sister hole influence," in *Proceedings of the ASME Turbo Expo 2012: Turbine Technical Conference and Exposition. Volume 4: Heat Transfer, Parts A and B*, pp. 1185–1196, Copenhagen, Denmark, 2012.

[17] H. Wu, H. Cheng, Y. Li, C. Rong, and S. Ding, "Effects of side hole position and blowing ratio on sister hole film cooling performance in a flat plate," *Applied Thermal Engineering*, vol. 93, pp. 718–730, 2016.

[18] J. Zhou, X. Wang, J. Li, and H. Lu, "Effects of diameter ratio and inclination angle on flow and heat transfer characteristics of sister holes film cooling," *International Communications in Heat and Mass Transfer*, vol. 110, article 104426, 2020.

[19] F. Yang and M. E. Taslim, "Experimental and numerical studies of the film cooling effectiveness downstream of a curved diffusion film cooling hole," *International Journal of Rotating Machinery*, vol. 2022, Article ID 9913692, 14 pages, 2022.

[20] F. Yang and M. E. Taslim, "Effects of diffusion film hole exit area on the film cooling effectiveness," *International Journal of Rotating Machinery*, vol. 2022, Article ID 5994933, 13 pages, 2022.

[21] S. K. Waye and D. G. Bogard, "High-resolution film cooling effectiveness measurements of axial holes embedded in a transverse trench with various trench configurations," *Journal of Turbomachinery*, vol. 129, no. 2, pp. 294–302, 2007.

[22] Y. Lu, A. Dhungel, S. V. Ekkad, and R. S. Bunker, "Effect of trench width and depth on film cooling from cylindrical holes embedded in trenches," *Journal of Turbomachinery*, vol. 131, no. 1, article 011003, 2009.

[23] H. I. Oguntade, G. E. Andrews, A. D. Burns, D. B. Ingham, and M. Pourkashanian, "Improved trench film cooling with shaped trench outlets," *Journal of Turbomachinery*, vol. 135, no. 2, article 021009, 2012.

[24] J. Wei, H. Zhu, C. Liu, H. Song, C. Liu, and T. Meng, "Experimental study on the film cooling characteristics of the cylindrical holes embedded in sine-wave shaped trench," in *Proceedings of the ASME Turbo Expo 2016: Turbomachinery Technical Conference and Exposition. Volume 5C: Heat Transfer*, Seoul, South Korea, 2016.

[25] S. D. Barahate and R. P. Vedula, "Film cooling performance measurement over a flat plate for a single row of holes embedded in an inclined trench," *International Journal of Thermal Sciences*, vol. 150, article 106215, 2020.

[26] Y. J. Song, S. H. Park, Y. J. Kang, and J. S. Kwak, "Effects of trench configuration on the film cooling effectiveness of a fan- shaped hole," *International Journal of Heat and Mass Transfer*, vol. 178, article 121655, 2021.

[27] X. Wu, X. Du, and C. Wang, "Study on film cooling performance of round hole embedded in different shaped craters and trenches," *Aerospace*, vol. 8, no. 6, p. 147, 2021.

[28] A. B. Bahambari, M. H. Kayhani, and M. Norouzi, "On the effect of geometry of w-wave trenches on film cooling performance of gas turbine blades," *Proceedings of the Institution of Mechanical Engineers, Part A: Journal of Power and Energy*, vol. 235, no. 7, pp. 1595–1618, 2021.

[29] K. R. Navarra, D. C. Rabe, S. D. Fonov, L. P. Goss, and C. Hah, "The application of pressure- and temperature-sensitive paints to an advanced compressor," *Journal of Turbomachinery*, vol. 123, no. 4, pp. 823–829, 2001.

[30] F. Baldino and M. E. Taslim, "Experimental Film Cooling Effectiveness of Multi-Row Patterns on Flat and Step-Down Surfaces," in *Proceedings of the ASME Turbo Expo 2019: Turbomachinery Technical Conference and Exposition. Volume 5B: Heat Transfer*, Phoenix, Arizona, USA, 2019.

[31] B. Johnson and H. Hu, "Measurement uncertainty analysis in determining adiabatic film cooling effectiveness by using pressure sensitive paint technique," *Journal of Turbomachinery*, vol. 138, no. 12, article 121004, 2016.

[32] S. J. Kline and F. A. McClintock, "Describing uncertainty in single-sample experiments," *Mechanical Engineering*, vol. 75, pp. 3–8, 1953.

[33] R. P. Schroeder and K. A. Thole, "Adiabatic effectiveness measurements for a baseline shaped film cooling hole," in *Proceedings of the ASME Turbo Expo 2014: Turbine Technical Conference and Exposition. Volume 5B: Heat Transfer*, Düsseldorf, Germany, 2014.